Data in Brief 46 (2023) 108892

Contents lists available at ScienceDirect

Data in Brief

journal homepage: www.elsevier.com/locate/dib

Data Article

Dataset for the new insights into methane hydrate inhibition with blends of vinyl lactam polymer and methanol, monoethylene glycol, or diethylene glycol as hybrid inhibitors

Anton P. Semenov[a,b,*], Yinghua Gong[a,b], Vladimir I. Medvedev[b], Andrey S. Stoporev[a,b], Vladimir A. Istomin[b,c], Vladimir A. Vinokurov[a,b], Tianduo Li[a,*]

[a] Shandong Provincial Key Laboratory of Molecular Engineering, School of Chemistry and Chemical Engineering, Qilu University of Technology (Shandong Academy of Sciences), Jinan 250353, China
[b] Department of Physical and Colloid Chemistry, Gubkin University, 65, Leninsky prospekt, Building 1, Moscow 119991, Russian Federation
[c] Skolkovo Institute of Science and Technology (Skoltech), Nobelya Str. 3, Moscow 121205, Russian Federation

ARTICLE INFO

Article history:
Received 20 December 2022
Accepted 6 January 2023
Available online 11 January 2023

Dataset link: Dataset for the new insights into methane hydrate inhibition with blends of vinyl lactam polymer and methanol, monoethylene glycol, or diethylene glycol as hybrid inhibitors (Original data)

Keywords:
Gas hydrates
Methane
Gas hydrate inhibitors
Phase equilibria
Hydrate nucleation
Gas uptake

ABSTRACT

Three-phase equilibrium conditions of vapor–aqueous solution–gas hydrate coexistence for the systems of CH_4–H_2O–organic thermodynamic inhibitor (THI) were experimentally determined. Hydrate equilibrium measurements for systems with methanol (MeOH), monoethylene glycol (MEG), and diethylene glycol (DEG) were conducted. Five concentrations of each inhibitor (maximum content 50 mass%) were studied in the pressure range of 4.9–8.4 MPa. The equilibrium temperature and pressure in the point of complete dissociation of methane hydrate during constant-rate heating combined with vigorous mixing of fluids (600 rpm) in a high-pressure vessel were determined. We compared our experimental points with reliable literature data. The coefficients of empirical equations are derived, which accurately describe hydrate equilibrium conditions for the studied systems. The effect of THI concentration and pressure on

DOI of original article: 10.1016/j.ces.2022.118387
* Corresponding authors at: Shandong Provincial Key Laboratory of Molecular Engineering, School of Chemistry and Chemical Engineering, Qilu University of Technology (Shandong Academy of Sciences), Jinan 250353, China.
E-mail addresses: semenov.a@gubkin.ru (A.P. Semenov), litianduo@qlu.edu.cn (T. Li).

https://doi.org/10.1016/j.dib.2023.108892

methane hydrate equilibrium temperature suppression was analyzed.
In the second stage, we studied the kinetics of methane hydrate nucleation/growth in systems containing a polymeric KHI (0.5 mass% of N-vinylpyrrolidone and N-vinylcaprolactam copolymer) in water or THI aqueous solution. For this, temperatures, pressures, and subcoolings of methane hydrate onset were measured by rocking cell tests (RCS6 rig, ramp cooling at 1 K/h). Gas uptake curves characterizing the methane hydrate crystallization kinetics in the polythermal regime were obtained.

Specifications Table

Subject	Chemistry
Specific subject area	Physical and Theoretical Chemistry
Type of data	Tables, figures
How the data were acquired	Three-phase equilibrium temperatures and pressures of vapor–aqueous solution–gas hydrate coexistence were determined for CH_4–H_2O–organic THI systems under isochoric conditions at 0.1 K/h linear heating and vigorous mixing of fluids. 600 mL high-pressure vessel GHA350 (PSL Systemtechnik, Germany) for hydrate equilibrium studies includes pressure, temperature transducers, mixing, and a thermostatic system. Pressure and temperature of complete dissociation of methane hydrate at constant-rate heating with simultaneous vigorous mixing (600 rpm) of fluids were taken as equilibrium conditions . The mixing system of the high-pressure vessel includes a four-bladed stirrer, a Minipower magnetic coupling (Premex, Switzerland), and an overhead stirrer Hei-TORQUE 400 Precision (Heidolph, Germany). Temperature control is carried out using CC 505 or Ministat 240 (both Huber, Germany), which pumps the coolant (ethanol) through the outer jacket of the high-pressure vessel. The GHA350 setup is connected to a PC with preinstalled WinGHA software for automatic control and recording of experimental data. Temperatures, pressures, and subcoolings of methane hydrate onset were measured by rocking cell tests using RCS6 rig (PSL Systemtechnik, Germany) with ramp cooling at 1 K/h. Nucleation and growth of methane hydrate in the CH_4–H_2O–KHI and CH_4–H_2O–KHI–THI systems at a fixed concentration of the polymeric kinetic inhibitor (0.5 mass%) in an aqueous solution were studied. The statistical significance of the results for each sample is ensured by measuring 12 to 24 hydrate onset events. The RCS6 contains six transparent sapphire cells with a volume of 20 mL, which are submerged in a thermostatic bath filled with coolant and connected to a thermostat Unistat 510 (Huber, Germany). Each cell has temperature/pressure sensors. A PC with WinRCS software controls the RCS6 rig. OriginPro 2022b software was used for experimental data processing and visualization.
Data format	Raw and analyzed
Description of data collection	Equilibrium conditions of the methane hydrate formation for CH_4–H_2O–organic THI systems at 10, 20, 30, 40, and 50 mass% of MeOH, MEG, and DEG in an aqueous solution were measured. Five equilibrium points were also obtained for the reference system CH_4–H_2O without the inhibitor. The mass of water or aqueous solution loaded into the high-pressure vessel GHA350 before each experimental series was constant (350 g). The measured equilibrium points for the studied systems cover the temperature range of 248–285 K and pressures of 4.9–8.4 MPa.

(*continued on next page*)

	Temperatures, pressures, and subcoolings of methane hydrate onset for the CH_4–H_2O–KHI and CH_4–H_2O–KHI–THI systems at a constant concentration of the polymeric kinetic inhibitor in an aqueous phase (0.5 mass%) and concentrations of each THI 0, 10, 20, 30, and 40 mass% were measured. The volume of the aqueous phase of the sample in each RCS6 cell was 10 mL. The initial gas pressure before the start of the first cooling–heating cycle was 8.1 MPa at 295 K.
Data source location	Gubkin University, Department of Physical and Colloid Chemistry. Moscow, Russia. 55.692232°N, 37.55487°E
Data accessibility	Repository name: Mendeley Data Data identification number: 10.17632/zwpgb24f9j.1 Direct URL to data: https://data.mendeley.com/datasets/zwpgb24f9j/1
Related research article	A.P. Semenov, Y. Gong, V.I. Medvedev, A.S. Stoporev, V.A. Istomin, V.A. Vinokurov, T. Li, New insights into methane hydrate inhibition with blends of vinyl lactam polymer and methanol, monoethylene glycol, or diethylene glycol as hybrid inhibitors, Chem. Eng. Sci. 268 (2023) 118387. https://doi.org/10.1016/j.ces.2022.118387. [1].

Value of the Data

- One can use the data for the systems CH_4–H_2O and CH_4–H_2O–organic THI (MeOH, MEG, DEG) to predict the thermodynamic stability of methane hydrate under given thermobaric conditions.
- Hydrate equilibrium data can be considered a reference for the CH_4–H_2O and CH_4–H_2O–organic THI (MeOH, MEG, DEG) systems in the studied range of temperatures, pressures, and alcohol concentrations.
- One can apply the data for comparative analysis of the anti-hydrate activity of MeOH, MEG, and DEG with other THIs in two concentration scales (mass% and mol%).
- The data on the thermodynamics and kinetics of methane hydrate formation in the presence of THI or THI/KHI mixtures is the basis for optimizing combined inhibitor formulations.
- The data contribute to a deeper understanding and further development of a hybrid inhibition strategy based on KHI/THI blends for gas hydrate prevention.

1. Objective

This dataset was generated as a result of work aimed at studying the regularities of methane hydrate inhibition by thermodynamic and kinetic mechanisms using hybrid inhibitors, which are mixtures of a commercial vinyl lactam polymer (KHI), and one of the alcohols, including methanol, monoethylene glycol, and diethylene glycol (THIs). The first part of the dataset is related to the study of gas–water solution–gas hydrate phase equilibrium in CH_4–H_2O–organic THI systems to obtain correlations for a quantitative description of the thermodynamic effect of these alcohols on methane hydrate inhibition. The first part of the dataset made it possible to quantitatively determine the thermodynamic contribution to the total inhibition effect for hybrid inhibitors KHI/THI. The second part of the dataset contains experimental data on the temperature, pressure, and subcooling of the methane hydrate onset (ramp cooling 1 K/h) for all samples. The second part of the dataset made it possible to establish how the addition of each alcohol to polymeric KHI affects the kinetics of nucleation and growth of methane hydrate, as well as to quantitatively characterize the contribution of the kinetic effect to the total inhibition effect for hybrid inhibitors KHI/THI.

2. Data Description

Fig. 1 shows a graph illustrating the evolution of temperature over time for measuring water freezing point at atmospheric pressure with a Pt100 temperature sensor of GHA350 after a calibration procedure. This reference was measured to confirm the reliability of the temperature sensor readings of high-pressure cell GHA350 and to evaluate the temperature stability. After the start of water crystallization from the supercooled state with stirring at 600 rpm, the temperature stabilizes at an average value of 0.022 °C with the maximum scatter not exceeding ±0.02 °C.

The measured equilibrium temperatures and pressures for the studied systems CH_4–H_2O–organic THI (MeOH, MEG, DEG) in the numerical form are in Table 1. Information on the correspondence between the sample name and its composition is available in the original research paper [1] (see Table 1). For each measured point, Table 1 of this work shows the corresponding value of methane hydrate equilibrium temperature suppression ΔT_h relative to the CH_4–H_2O system without inhibitor at the indicated equilibrium pressure. A comparison of the obtained equilibrium points with literature data for the system of CH_4–MeOH–H_2O [2–5], CH_4–MEG–H_2O [3,5–7], and CH_4–DEG–H_2O [8–10] is shown in Figs. 2, 3, and 4, respectively.

The numerical magnitudes of the coefficients obtained by approximating the experimental points by the empirical function $\ln P = A + B/T$ are collected in Table 2. The graphs in Fig. 5 show the dependence of the coefficient B of the two-parameter function on the concentration of each thermodynamic inhibitor in solution. The fitting results of the experimental equilibrium points by the same empirical function are in Fig. 6. This figure separately shows panels with plots of model residuals for all systems and samples depending on the approximated value of $\ln P$. The approximation results by an alternative three-parameter empirical function $\ln P = A + B/T + C \cdot \ln T$ are shown in Table 3 and Fig. 7.

The two-dimensional plots in Figs. 8 and 9 demonstrate the relationship between the methane hydrate equilibrium temperature suppression, the pressure, and the concentration of the thermodynamic inhibitors (MeOH, MEG, and DEG) in the solution. Tables 4–6 contain the

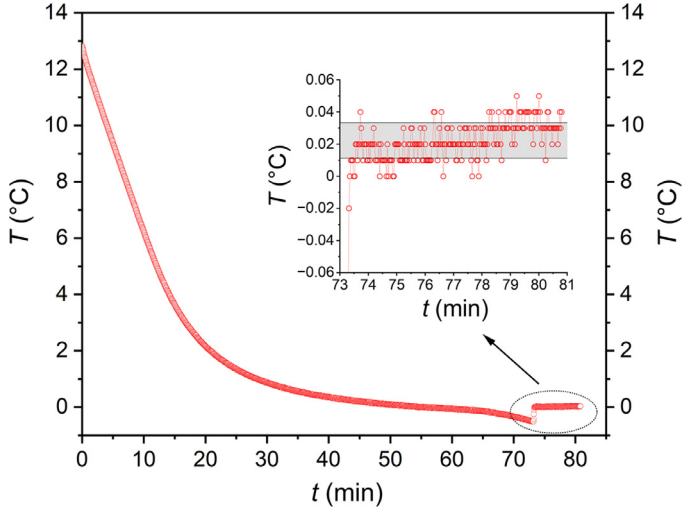

Fig. 1. The temperature in the GHA350 autoclave versus time when measuring the freezing point of deionized water; after the onset of water crystallization from the supercooled state (73 min), the temperature reaches a plateau with a mean value and a standard deviation of 0.022 ± 0.011 °C (the area highlighted in gray in the inset).

Table 1
Experimental data on CH_4 hydrate equilibrium conditions for THIs aqueous solutions; the exact composition of aqueous solutions is in the original research paper [1] (see Table 1); heating rate near the equilibrium point was 0.1 K/h unless otherwise noted.

Sample	T / K[a]	P / MPa [b]	ΔT_h / K	Sample	T / K [a]	P / MPa [b]	ΔT_h / K	Sample	T / K [a]	P / MPa [b]	ΔT_h / K
DW	279.26	4.77	0	MEG10	277.50	4.99	2.20	DEG10	278.49	5.04	1.31
	281.11	5.78	0		279.21	5.99	2.24		280.14	5.99	1.31
	282.62	6.77	0		280.55	6.86	2.18		281.35	6.83	1.33
	283.87	7.78	0		281.26	7.43	2.21		282.09	7.40	1.34
	285.01	8.84	0		282.14	8.18	2.20		282.97	8.18	1.36
Me10	275.25	4.97	4.41	MEG20	274.33	5.02	5.43	DEG20	276.33	4.99	3.38
	277.01	5.99	4.44		276.10	6.04	5.44		278.00	5.94	3.38
	278.36	6.90	4.43		277.29	6.87	5.45		279.38	6.88	3.38
	279.05	7.45	4.44		278.04	7.45	5.45		280.10	7.45	3.39
	279.90	8.19	4.44		278.91	8.21	5.46		280.98	8.20	3.38
Me20	269.87	4.99	9.84	MEG30	270.34	4.97	9.32	DEG30	273.52	4.95	6.10
	271.63	5.99	9.83		272.10	5.97	9.32		275.16	5.87	6.11
	272.95	6.91	9.85		273.41	6.88	9.35		275.17	5.86	6.08
	273.64	7.43	9.83		274.15	7.46	9.35		276.51	6.86	6.22
	274.45	8.15	9.86		274.96	8.15	9.34		277.31	7.46	6.20
Me30	263.24	4.97	16.41	MEG40	264.67	4.94	14.92		278.12	8.16	6.20
	265.00	5.94	16.38		266.50	5.96	14.91	DEG40	269.66	4.97	10.01
	266.58	7.01	16.35		267.94	6.97	14.93		271.14[d]	5.83[d]	10.06[d]
	267.18	7.50	16.37		268.56	7.43	14.91		271.15[d]	5.85[d]	10.08[d]
	267.94	8.14	16.35		269.41	8.18	14.93		271.20	5.84	10.02
Me40	256.07	4.94	23.54	MEG50	257.50	4.99	22.20		272.47	6.80	10.18
	257.70	5.84	23.51		259.21	5.98	22.23		273.39	7.51	10.18
	257.71	5.87	23.56		260.51	6.89	22.27		274.25	8.24	10.16
	259.33	6.91	23.47		261.07	7.36	22.30	DEG50	263.55	4.93	16.04
	259.38	6.93	23.45		262.11	8.27	22.32		265.45	6.03	16.06
	260.01	7.49	23.53						266.68	6.88	16.08
	260.98	8.35	23.54						267.39	7.47	16.12
Me50	248.34	4.99	31.36						268.22	8.20	16.13
	249.99	5.93	31.37								
	250.01[c]	5.94[c]	31.36[c]								
	251.41	6.90	31.37								
	252.25	7.52	31.31								
	252.26	7.53	31.34								
	252.71	7.99	31.42								

[a] Expanded uncertainty of temperature measurements is 0.1 K ($k = 2$).
[b] Expanded uncertainty of pressure measurements is 0.02 MPa ($k = 2$).
[c] Heating rate near the equilibrium point was 0.5 K/h.
[d] Step heating near the equilibrium point (each step is 0.2 K with keeping for 3 h for equilibration).

results of surface fitting by Eq. 4 from ref. [11] ΔT_h as a function of pressure and concentration of each organic THI on two different scales (mass%, mol%). Table 7 presents the interpolated values ΔT_h (Eq. (4) from Ref. [11]) for methanol, monoethylene glycol, and diethylene glycol at a pressure of 6 MPa and a mass fraction of each of the alcohols 10,20,30,40, and 50 mass%. In the three columns to the right of this Table, the interpolated values ΔT_h are normalized to the same for MeOH, which makes it possible to see the change in the anti-hydrate activity of MEG and DEG relative to MeOH for the indicated concentrations of inhibitors.

The experimental dataset obtained in the study of the kinetics of nucleation and growth of methane hydrate in the systems of CH_4–H_2O–KHI and CH_4–H_2O–KHI–THI can be found in Table 8. Here, for each sample, the measured temperatures, pressures, and subcoolings of methane hydrate onset in polythermal mode (cooling 1 K/h), together with the mean and stan-

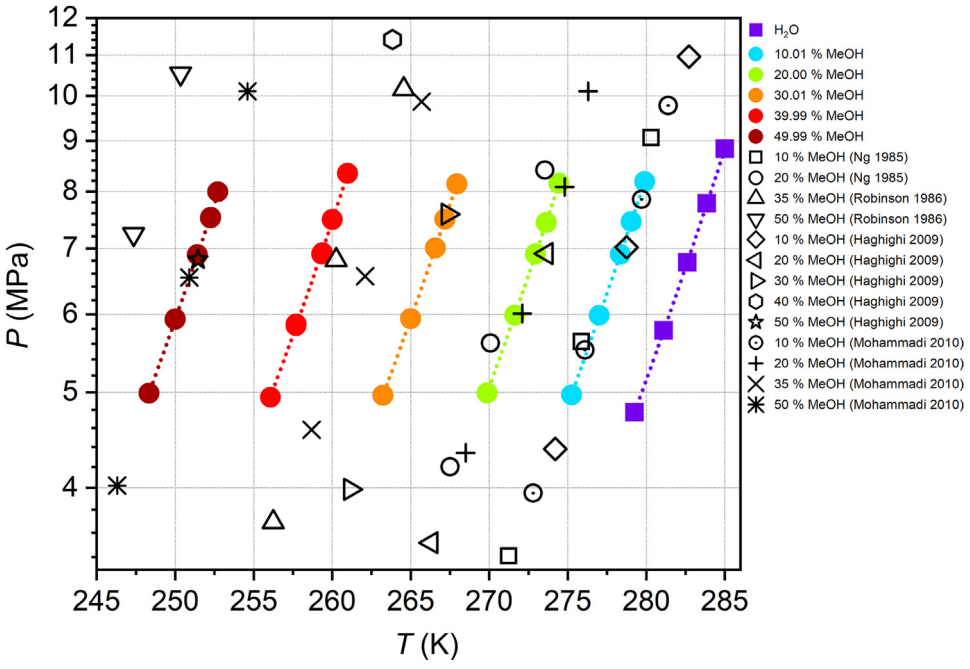

Fig. 2. Comparison of experimental results on the methane hydrate equilibrium for CH_4–MeOH–H_2O system, obtained in this work (color symbols), with literature data (black-edge symbols) [2–5]; dotted lines – interpolation of our data by the equation ln $P=A+B/T+C\cdot\ln T$ (coefficients are in Table 3); the concentration of MeOH in aqueous solution is in mass%.

Table 2
Approximation results of experimental data on methane hydrate equilibrium conditions (V-L_w-H) in the systems of CH_4–H_2O–THI (where THI = methanol, MEG, DEG) by equation $\ln P=A+B/T$; the exact composition of each aqueous solution is in the original research paper [1] (see Table 1).

#	Solution sample	*A*		*B*, K		
		Value	Standard Error	Value	Standard Error	Adjusted R^2
1	DW	32.08	0.43	−8523.68	121.83	0.99918
2	Me10	31.58	0.27	−8251.48	73.88	0.99968
3	Me20	30.90	0.37	−7906.86	100.38	0.99936
4	Me30	29.77	0.34	−7415.49	89.53	0.99942
5	Me40	29.22	0.46	−7075.33	119.85	0.99828
6	Me50	28.54	0.34	−6689.13	84.68	0.99904
7	MEG10	31.55	0.31	−8310.66	85.59	0.99958
8	MEG20	31.49	0.29	−8197.38	79.98	0.99962
9	MEG30	31.05	0.27	−7960.15	74.39	0.99965
10	MEG40	30.27	0.33	−7590.41	88.48	0.99946
11	MEG50	30.30	0.36	−7389.34	94.86	0.99934
12	DEG10	32.13	0.37	−8498.47	105.20	0.99939
13	DEG20	31.54	0.28	−8270.80	77.57	0.99965
14	DEG30	32.12	0.42	−8349.00	115.82	0.99904
15	DEG40	32.11	0.33	−8226.76	90.77	0.99927
16	DEG50	30.70	0.39	−7671.11	103.49	0.99927

Table 3
Approximation results of experimental data on methane hydrate equilibrium conditions (V-L_w-H) in the systems of CH_4–H_2O–THI (where THI = methanol, MEG, DEG) by equation $\ln P = A + B/T + C \cdot \ln T$; the exact composition of each aqueous solution is in the original research paper [1] (see Table 1).

		A		*B*, K		*C*		
#	Solution sample	Value	Standard Error	Value	Standard Error	Value	Standard Error	Adjusted R^2
1	DW	−1591.58	162.60	60,432.59	6905.75	244.44	24.48	0.99998
2	Me10	−1158.51	262.38	41,593.77	10,989.38	179.61	39.60	0.99996
3	Me20	−1641.18	274.52	60,963.95	11,307.12	253.11	41.55	0.99995
4	Me30	−1516.38	190.10	54,962.77	7669.32	234.91	28.88	0.99997
5	Me40	−1912.05	634.73	69,479.81	25,031.03	296.16	96.83	0.99936
6	Me50	−1285.77	756.52	43,797.37	29,060.48	201.46	115.96	0.99932
7	MEG10	−1051.07	672.45	37,345.05	28,358.39	163.19	101.37	0.99972
8	MEG20	−1296.69	53.25	47,268.85	2223.71	200.56	8.04	1.00000
9	MEG30	−1195.29	196.06	42,628.59	8087.73	185.58	29.67	0.99997
10	MEG40	−1380.45	310.74	49,585.28	12,594.00	214.16	47.17	0.99993
11	MEG50	−1476.37	215.13	52,267.48	8518.19	229.69	32.80	0.99996
12	DEG10	−1764.44	68.79	67,475.24	2908.88	270.68	10.36	1.00000
13	DEG20	−1272.24	94.31	46,517.07	3963.07	196.65	14.22	0.99999
14	DEG30	−1498.91	882.47	55,447.67	36,771.71	231.28	133.31	0.99936
15	DEG40	−843.18	834.58	27,816.42	34,367.29	132.50	126.34	0.99928
16	DEG50	−1632.05	248.51	59,471.43	10,034.81	252.59	37.75	0.99995

Table 4
Results of surface fitting (Eq. (4) from Ref. [11]) of our experimental data on methane hydrate equilibrium temperature suppression ΔT_h (system CH_4–MeOH–H_2O) as a function of methanol concentration in aqueous solution (0–50 mass% or 0–35.98 mol%) and pressure in the system (4.9–8.3 MPa).

Coefficient	mass% scale	mol% scale
b_1	186.4568749	120.1802644
b_2	2.8800918	2.3772094
b_3	−0.0074353	−0.0550439
b_4	$-5.1503644 \cdot 10^{-5}$	$4.2319551 \cdot 10^{-4}$
b_5	0.0021068	0.005798
b_6	$-1.6218453 \cdot 10^{-5}$	$-4.4299892 \cdot 10^{-5}$
b_7	$1.2155107 \cdot 10^{-6}$	$3.31739 \cdot 10^{-6}$
Adjusted R^2	0.99999	0.99999
Average absolute deviation (K)	0.03	0.03
Average absolute relative deviation (%)	0.28	0.29

Table 5
Results of surface fitting (Eq. (4) from Ref. [11]) of our experimental data on methane hydrate equilibrium temperature suppression ΔT_h (system CH_4–MEG–H_2O) as a function of MEG concentration in aqueous solution (0–50 mass% or 0–22.49 mol%) and pressure in the system (4.9–8.3 MPa).

Coefficient	mass% scale	mol% scale
b_1	147.7441129	75.9040683
b_2	3.6037371	1.8840591
b_3	−0.0248299	−0.0128072
b_4	$7.5163777 \cdot 10^{-4}$	$-1.0551385 \cdot 10^{-4}$
b_5	0.0012316	0.0088987
b_6	$4.881568 \cdot 10^{-7}$	$4.7449668 \cdot 10^{-6}$
b_7	$8.1330386 \cdot 10^{-8}$	$4.9554775 \cdot 10^{-7}$
Adjusted R^2	0.99991	0.99990
Average absolute deviation (K)	0.06	0.06
Average absolute relative deviation (%)	1.10	1.36

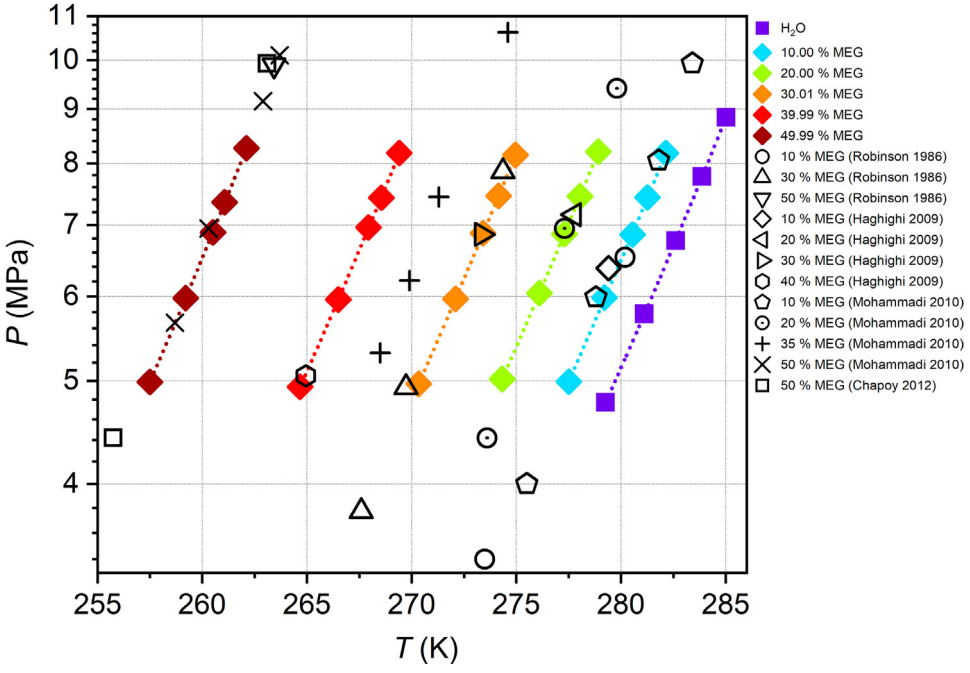

Fig. 3. Comparison of experimental results on the methane hydrate equilibrium for CH_4–MEG–H_2O system, obtained in this work (color symbols), with literature data (black-edge symbols) [3,5–7]; dotted lines – interpolation of our data by the equation $\ln P = A + B/T + C \cdot \ln T$ (coefficients are in Table 3); the concentration of MEG in aqueous solution is in mass%.

Table 6
Results of surface fitting (Eq. 4 from ref. [11]) of our experimental data on methane hydrate equilibrium temperature suppression ΔT_h (system CH_4–DEG–H_2O) as a function of DEG concentration in aqueous solution (0–50 mass% or 0–14.51 mol%) and pressure in the system (4.9–8.3 MPa).

Coefficient	mass% scale	mol% scale
b_1	67.840763	26.181747
b_2	3.8008564	2.3571797
b_3	−0.0676243	−0.1331213
b_4	0.001223	0.0043466
b_5	0.0013418	0.0244815
b_6	$-7.6841481 \cdot 10^{-6}$	$-1.3993317 \cdot 10^{-4}$
b_7	$8.9602628 \cdot 10^{-7}$	$1.6331902 \cdot 10^{-5}$
Adjusted R^2	0.99999	0.99998
Average absolute deviation (K)	0.01	0.02
Average absolute relative deviation (%)	0.37	0.66

dard deviations of these values, are shown. A complete description of sample solutions with a kinetic inhibitor and their composition is in the original research paper [1] (see Table 2). Based on the experimental $P(T)$-trajectories (see https://data.mendeley.com/datasets/zwpgb24f9j/1) for each sample, the calculated amount of consumed methane during the hydrate growth was obtained (Fig. 10). The calculation details are discussed in section 2.3.2 of the original research paper [1]. The average methane uptake rates r during hydrate growth for each system (Fig. 11) were derived by differentiating the gas uptake curves (Fig. 10) over time.

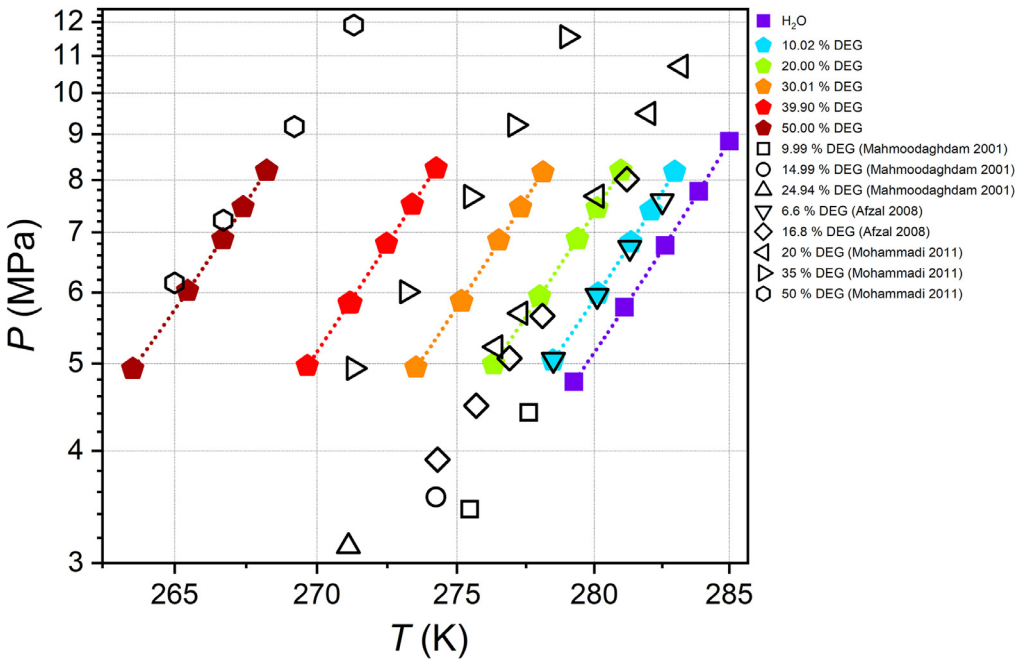

Fig. 4. Comparison of experimental results on the methane hydrate equilibrium for CH_4–DEG–H_2O system, obtained in this work (color symbols), with literature data (black-edge symbols) [8–10]; dotted lines – interpolation of our data by the equation $\ln P = A + B/T + C \cdot \ln T$ (coefficients are in Table 3); the concentration of DEG in aqueous solution is in mass%.

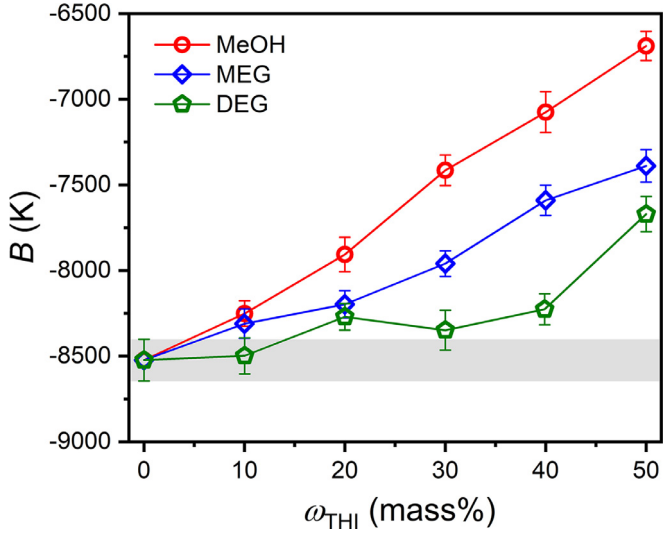

Fig. 5. Coefficient B (Eq. $\ln P = A + B/T$) as a function of the mass fraction of thermodynamic inhibitor in aqueous solution; markers and error bars correspond to the value and standard error of B in Table 2 (gray-filled area shows pure water mean value and standard deviation).

Table 7
Comparison of interpolated values of CH_4 hydrate equilibrium temperature suppression ΔT_h at 6 MPa for methanol, monoethylene glycol, and diethylene glycol (Eq. (4) from Ref. [11] and coefficients are in Tables 4–6 for mass% scale) and the same values normalized by methanol thermodynamic effect $\Delta T_{h\ MeOH}$.

ω_{THI}, mass%	P, MPa	ΔT_h, K			$\Delta T_{h\ THI} / \Delta T_{h\ MeOH}$		
		MeOH	MEG	DEG	MeOH	MEG	DEG
10.00	6.00	4.40	2.25	1.33	1.000	0.512	0.303
20.00		9.88	5.34	3.36	1.000	0.541	0.340
30.00		16.31	9.42	6.14	1.000	0.578	0.376
40.00		23.53	14.86	10.09	1.000	0.632	0.429
50.00		31.36	22.26	16.05	1.000	0.710	0.512

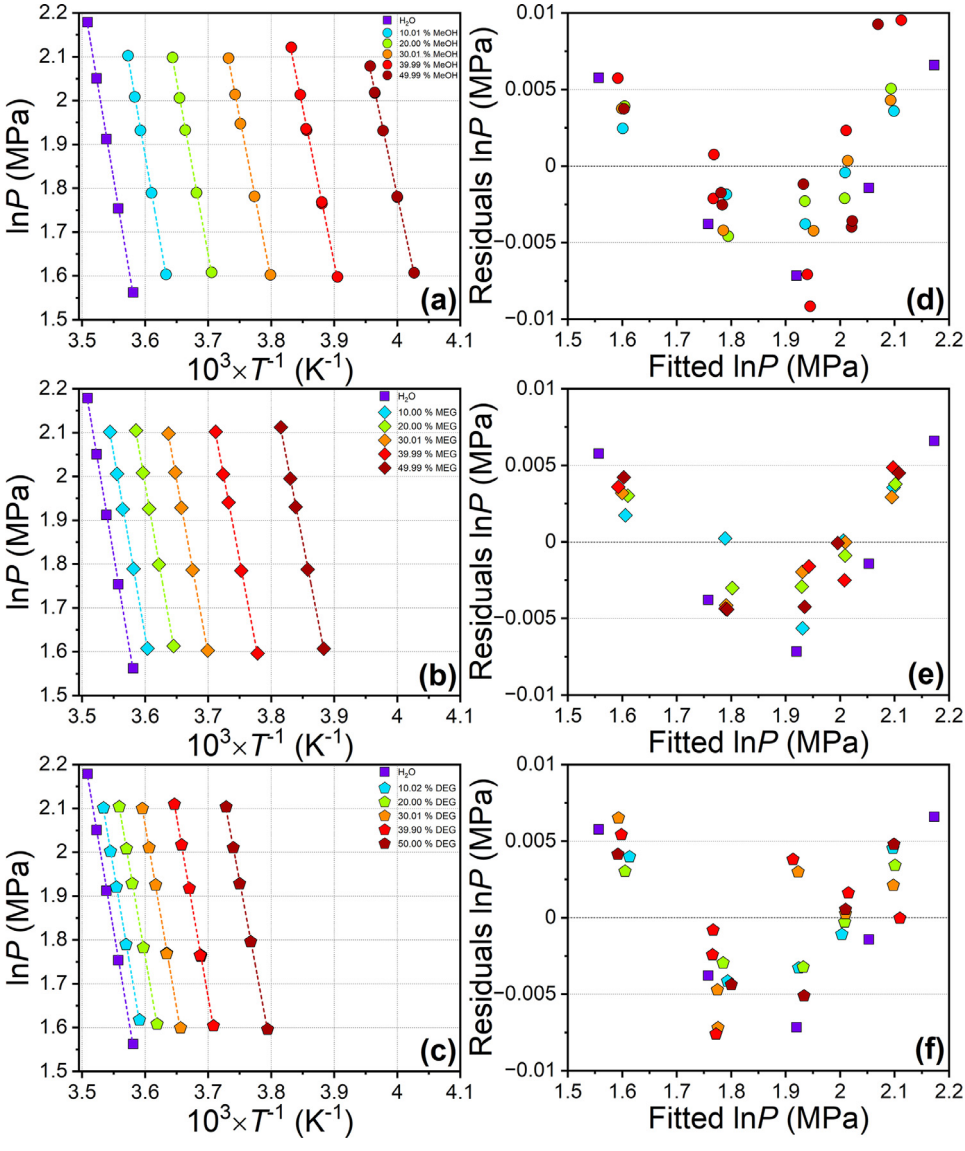

Fig. 6. (a-c) Experimental data on methane hydrate equilibrium conditions in semi-logarithmic coordinates (markers) and linear approximations ln $P=A+B/T$ (dashed lines); concentrations of methanol, MEG, and DEG in aqueous solution are in mass%; (d–f) model residuals as a function of the approximated logarithmic pressure value for all studied concentrations of THIs.

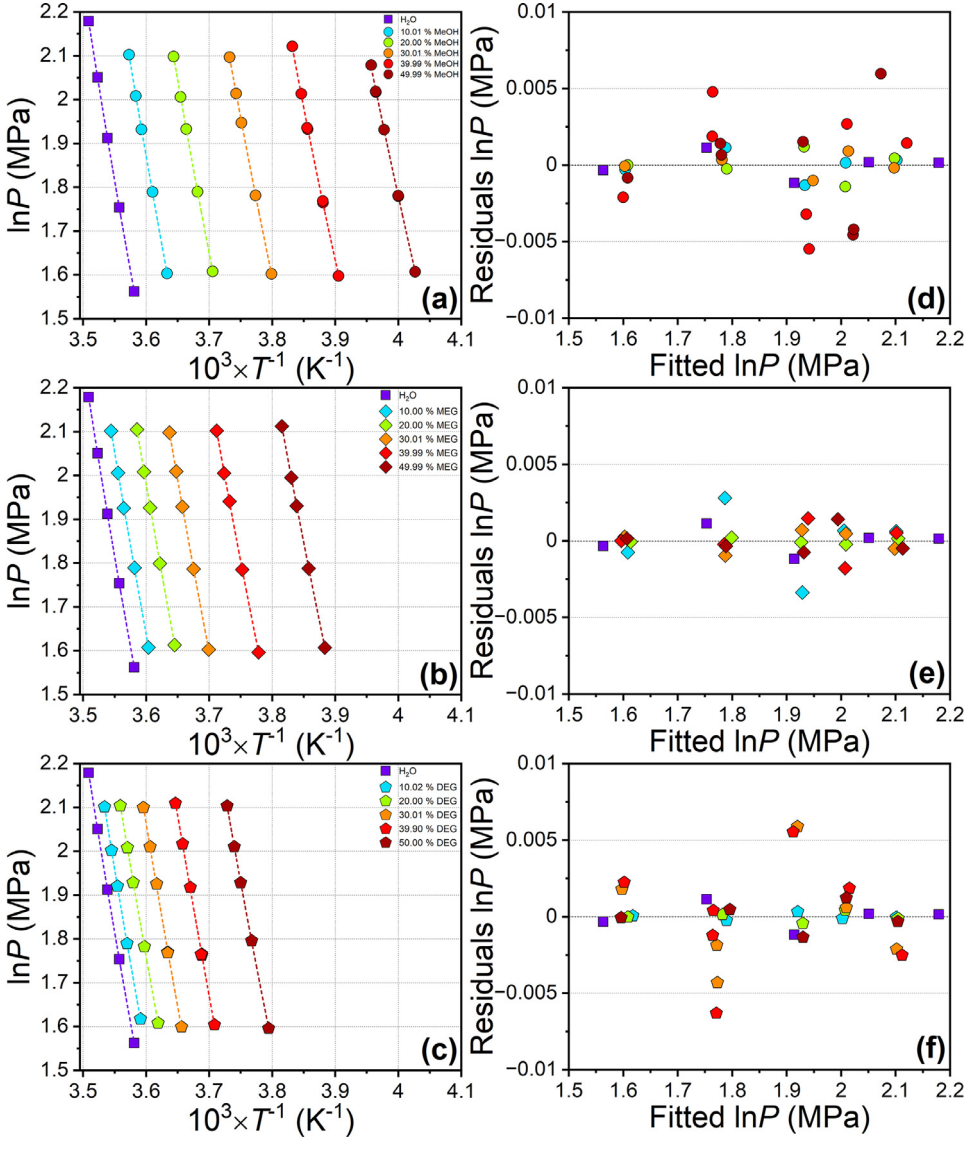

Fig. 7. (a–c) Experimental data on methane hydrate equilibrium conditions in semi-logarithmic coordinates (markers) and approximations by equation $\ln P = A + B/T + C \cdot \ln T$ (dashed lines); concentrations of methanol, MEG, and DEG in aqueous solution are in mass%; (d–f) model residuals as a function of the approximated logarithmic pressure value for all studied concentrations of THIs.

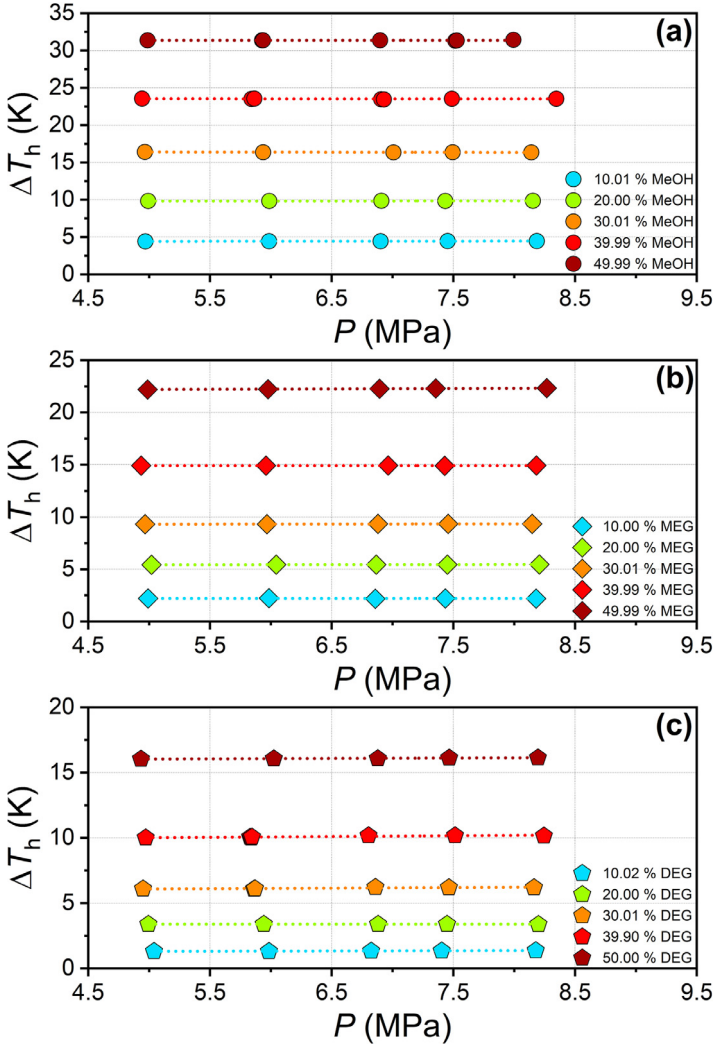

Fig. 8. Methane hydrate equilibrium temperature suppression ΔT_h depending on the equilibrium pressure for aqueous solutions of methanol (a), MEG (b), DEG (c); markers – experiment, dotted lines – linear approximation; the concentrations of methanol, MEG, and DEG in aqueous solution are in mass%.

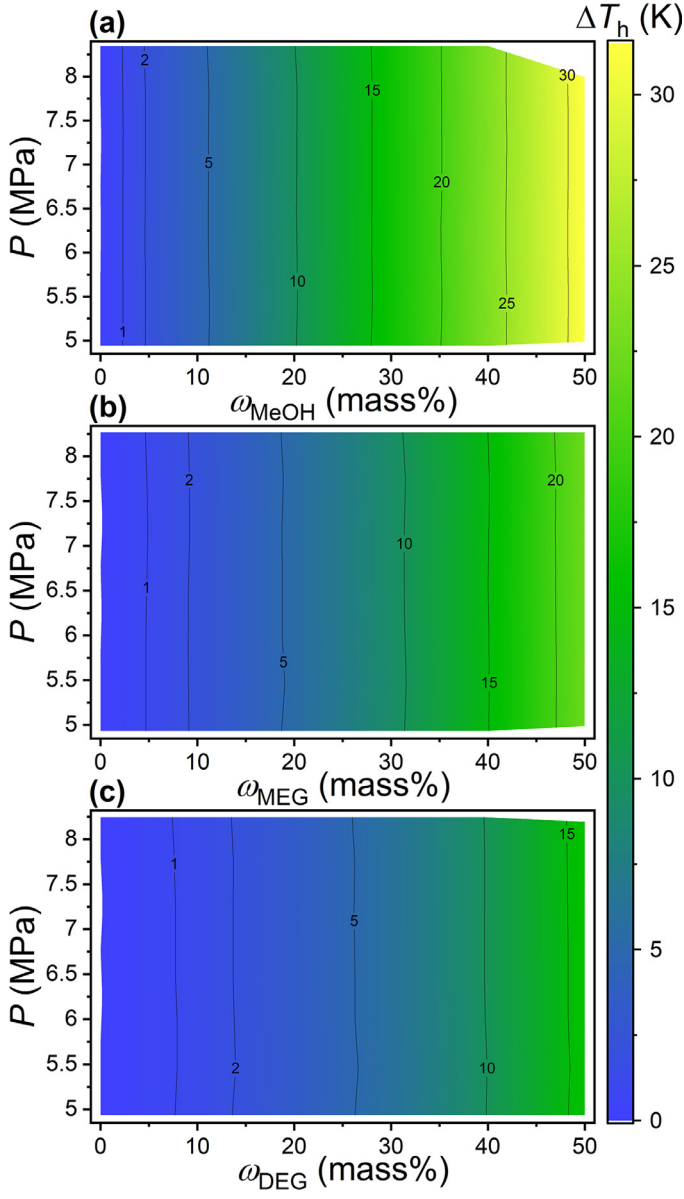

Fig. 9. Colored contours of methane hydrate equilibrium temperature suppression ΔT_h for entire pressure and concentration ranges of methanol (a), MEG (b), DEG (c) aqueous solutions.

Table 8
Experimental data on methane hydrate onset temperatures, pressures, and subcooling (rocking cell experiments, cooling rate of 1 K/h, initial methane pressure of 8.1 MPa at 295 K, total 215 hydrate onset events); the mean and standard deviation of the indicated values for each sample are shown in bold); the exact composition of each aqueous solution is in the original research paper [1] (see Table 2).

#	Sample ID and number of hydrate onset events	T_{onset}, K	P_{onset}, MPa	ΔT_{onset}, K
1	DW (18 events)	282.15	7.51	1.41
		281.35	7.46	2.15
		280.55	7.51	3.01
		281.95	7.56	1.67
		280.85	7.5	2.70
		281.75	7.52	1.83
		280.75	7.47	2.77
		280.15	7.41	3.29
		280.35	7.49	3.19
		281.15	7.54	2.45
		280.15	7.46	3.35
		281.85	7.53	1.74
		281.05	7.46	2.45
		280.05	7.41	3.39
		280.65	7.51	2.91
		280.45	7.51	3.11
		279.65	7.43	3.82
		281.15	7.49	2.39
		280.89 ± 0.72	**7.49 ± 0.04**	**2.65 ± 0.68**
2	0.5KHI (12 events)	277.55	7.37	5.84
		277.65	7.39	5.77
		277.95	7.4	5.48
		278.35	7.4	5.08
		278.05	7.37	5.34
		277.65	7.4	5.78
		277.35	7.35	6.02
		277.25	7.38	6.15
		277.15	7.37	6.24
		277.65	7.37	5.74
		277.45	7.35	5.92
		277.05	7.37	6.34
		277.59 ± 0.38	**7.38 ± 0.02**	**5.81 ± 0.37**
3	0.5KHI/Me10 (18 events)	274.65	7.26	4.17
		274.95	7.27	3.88
		274.65	7.26	4.17
		274.65	7.28	4.19
		274.45	7.22	4.32
		274.95	7.32	3.94
		274.95	7.23	3.83
		274.55	7.24	4.24
		274.65	7.26	4.17
		274.75	7.27	4.08
		274.65	7.23	4.13
		274.85	7.31	4.03
		274.75	7.26	4.07
		274.65	7.25	4.15
		274.55	7.25	4.25
		274.85	7.27	3.98
		274.25	7.21	4.50
		274.65	7.3	4.22
		274.69 ± 0.18	**7.26 ± 0.03**	**4.13 ± 0.16**
4	0.5KHI/Me20 (12 events)	270.05	7.08	3.13
		270.55	7.11	2.67
		270.35	7.1	2.86

(*continued on next page*)

Table 8 (*continued*)

#	Sample ID and number of hydrate onset events	T_{onset}, K	P_{onset}, MPa	ΔT_{onset}, K
		270.55	7.13	2.70
		270.35	7.12	2.89
		270.35	7.17	2.95
		270.65	7.08	2.53
		270.55	7.07	2.62
		270.55	7.08	2.63
		270.95	7.1	2.26
		270.65	7.11	2.57
		270.85	7.15	2.42
		270.53 ± 0.24	**7.11 ± 0.03**	**2.69 ± 0.24**
5	0.5KHI/Me30 (12 events)	263.95	6.85	2.41
		263.55	6.85	2.81
		263.65	6.88	2.75
		264.25	6.89	2.16
		263.55	6.88	2.85
		263.75	6.94	2.73
		264.15	6.86	2.22
		263.45	6.84	2.89
		263.65	6.88	2.75
		264.05	6.87	2.33
		264.25	6.9	2.17
		263.45	6.93	3.01
		263.81 ± 0.31	**6.88 ± 0.03**	**2.59 ± 0.31**
6	0.5KHI/Me40 (12 events)	256.45	6.58	2.41
		256.05	6.56	2.78
		256.45	6.62	2.46
		256.15	6.57	2.69
		255.75	6.58	3.11
		255.05	6.63	3.88
		255.95	6.56	2.88
		256.55	6.58	2.31
		255.95	6.6	2.93
		256.45	6.58	2.41
		254.25	6.52	4.52
		255.35	6.64	3.59
		255.87 ± 0.69	**6.59 ± 0.03**	**3.00 ± 0.68**
7	0.5KHI/MEG10 (18 events)	274.25	7.3	6.88
		274.25	7.31	6.89
		273.35	7.23	7.69
		274.45	7.31	6.69
		273.35	7.24	7.70
		274.05	7.4	7.20
		274.15	7.3	6.98
		274.15	7.31	6.99
		274.35	7.33	6.81
		273.65	7.29	7.46
		273.65	7.25	7.41
		274.15	7.41	7.11
		274.65	7.32	6.50
		274.05	7.3	7.08
		273.85	7.3	7.28
		274.25	7.3	6.88
		273.65	7.25	7.41
		274.15	7.4	7.10
		274.02 ± 0.36	**7.31 ± 0.05**	**7.11 ± 0.33**
8	0.5KHI/MEG20 (12 events)	270.95	7.24	6.83
		270.35	7.21	7.39
		270.85	7.25	6.94

(*continued on next page*)

Table 8 (*continued*)

#	Sample ID and number of hydrate onset events	T_{onset}, K	P_{onset}, MPa	ΔT_{onset}, K
		270.65	7.23	7.11
		269.85	7.17	7.84
		270.55	7.34	7.35
		271.05	7.24	6.73
		270.15	7.2	7.58
		270.95	7.25	6.84
		270.55	7.22	7.20
		270.65	7.2	7.08
		270.85	7.35	7.06
		270.62 ± 0.36	**7.24 ± 0.05**	**7.16 ± 0.33**
9	0.5KHI/MEG30 (11 events)	265.55	7.00	8.01
		265.55	7.00	8.01
		265.55	7.01	8.03
		265.85	6.99	7.70
		265.55	7.13	8.18
		265.65	7.00	7.91
		265.55	7.00	8.01
		264.85	6.82	8.47
		265.95	7.02	7.64
		265.95	6.99	7.60
		265.65	7.14	8.10
		265.60 ± 0.30	**7.01 ± 0.08**	**7.97 ± 0.25**
10	0.5KHI/MEG40 (24 events)	258.65	6.72	8.98
		258.15	6.68	9.42
		258.85	6.77	8.85
		257.95	6.69	9.64
		258.05	6.69	9.54
		258.45	6.87	9.38
		258.45	6.71	9.16
		258.15	6.67	9.41
		257.65	6.73	9.99
		258.15	6.7	9.45
		258.55	6.72	9.08
		258.45	6.86	9.37
		258.95	6.72	8.68
		258.55	6.68	9.02
		259.05	6.77	8.65
		258.45	6.71	9.16
		258.85	6.72	8.78
		258.65	6.86	9.17
		258.55	6.71	9.06
		258.45	6.67	9.11
		259.05	6.77	8.65
		258.45	6.71	9.16
		257.65	6.68	9.92
		258.35	6.85	9.45
		258.44 ± 0.38	**6.74 ± 0.06**	**9.21 ± 0.36**
11	0.5KHI/DEG10 (24 events)	276.05	7.34	5.88
		275.75	7.34	6.18
		275.25	7.33	6.67
		275.55	7.32	6.35
		275.75	7.31	6.14
		275.15	7.44	6.91
		275.55	7.33	6.37
		275.35	7.33	6.57
		275.75	7.35	6.19
		275.15	7.31	6.74
		276.25	7.33	5.67
		274.75	7.42	7.28

(*continued on next page*)

Table 8 (*continued*)

#	Sample ID and number of hydrate onset events	T_{onset}, K	P_{onset}, MPa	ΔT_{onset}, K
		276.05	7.35	5.89
		275.35	7.33	6.57
		275.65	7.34	6.28
		275.25	7.32	6.65
		275.45	7.3	6.43
		274.95	7.43	7.09
		276.75	7.37	5.22
		274.75	7.3	7.13
		275.65	7.34	6.28
		275.45	7.32	6.45
		275.55	7.3	6.33
		275.25	7.44	6.81
		275.52 ± 0.46	**7.35 ± 0.04**	**6.42 ± 0.47**
12	0.5KHI/DEG20 (12 events)	273.15	7.23	6.68
		272.15	7.19	7.63
		272.55	7.21	7.26
		272.55	7.21	7.26
		272.65	7.18	7.12
		273.25	7.35	6.73
		272.35	7.21	7.46
		272.15	7.21	7.66
		272.55	7.23	7.28
		272.65	7.21	7.16
		272.05	7.17	7.70
		272.95	7.35	7.03
		272.58 ± 0.38	**7.23 ± 0.06**	**7.25 ± 0.33**
13	0.5KHI/DEG30 (18 events)	269.05	7.12	7.81
		268.85	7.13	8.02
		268.55	7.12	8.31
		268.15	7.1	8.69
		268.65	7.09	8.17
		268.95	7.24	8.06
		268.35	7.1	8.49
		268.45	7.11	8.40
		268.25	7.12	8.61
		269.15	7.13	7.72
		267.95	7.07	8.85
		268.15	7.22	8.84
		268.75	7.11	8.10
		268.15	7.1	8.69
		268.25	7.12	8.61
		268.45	7.11	8.40
		267.85	7.06	8.93
		268.75	7.24	8.26
		268.48 ± 0.38	**7.13 ± 0.05**	**8.39 ± 0.36**
14	0.5KHI/DEG40 (12 events)	262.75	6.85	9.79
		261.85	6.81	10.64
		263.15	6.89	9.44
		262.35	6.83	10.16
		263.05	6.84	9.48
		262.65	6.99	10.07
		262.85	6.88	9.73
		262.85	6.87	9.72
		262.95	6.9	9.66
		263.15	6.88	9.43
		262.85	6.85	9.69
		262.95	7.02	9.81
		262.78 ± 0.37	**6.88 ± 0.06**	**9.80 ± 0.35**

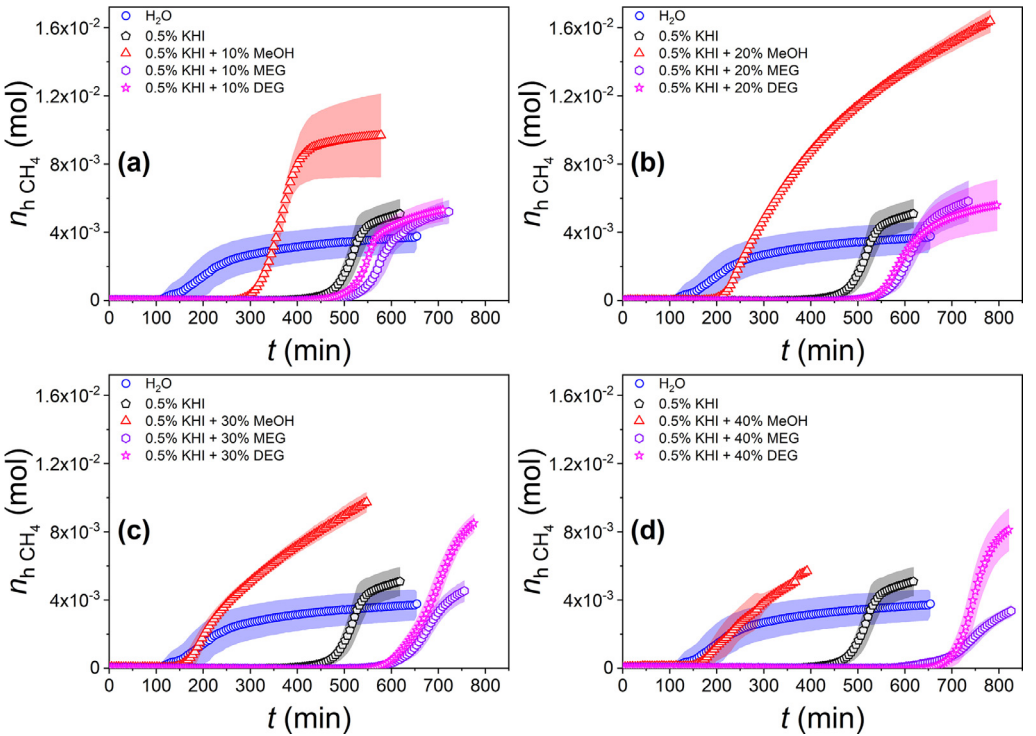

Fig. 10. (a)–(d) Average curves of methane uptake as a function of time upon ramp cooling at 1 K/h for pure water, polymeric KHI, and blends KHI+THI; markers and color fill for each sample correspond to the average values and standard deviation of $n_{h\ CH4}$; zero time coincides with the intersection of the experimental $P(T)$-trajectory and the hydrate equilibrium curve; values in legend are in mass%.

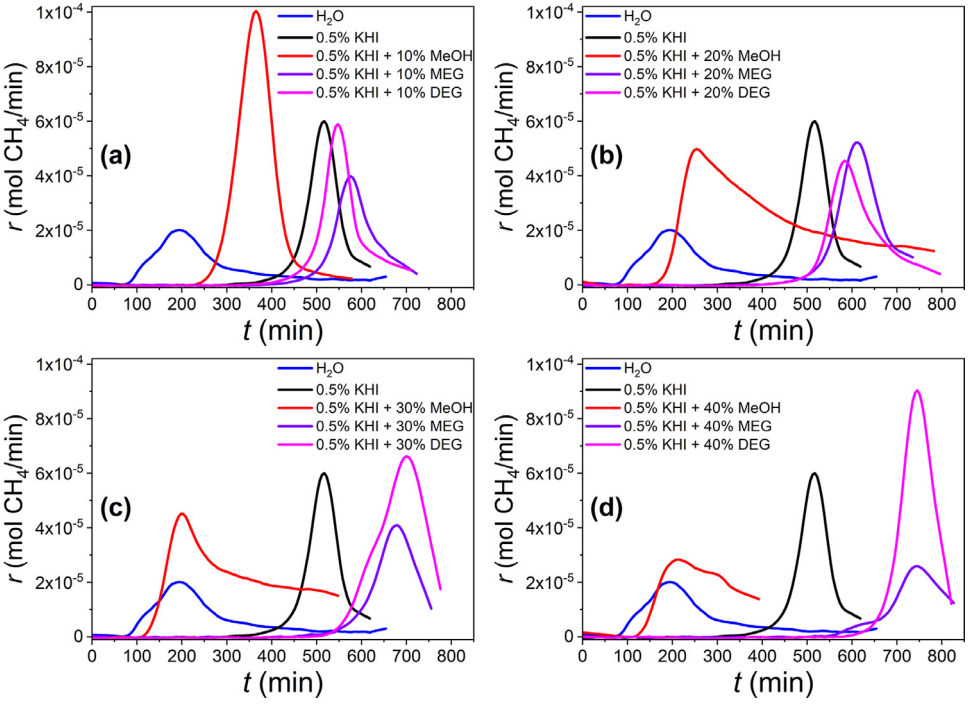

Fig. 11. (a–d) Average methane uptake rate r during hydrate formation as a function of time upon ramp cooling at 1 K/h for pure water, polymeric KHI, and blends KHI+THI; zero time coincides with the intersection of the experimental $P(T)$-trajectory and the hydrate equilibrium curve; values in legend are in mass%.

3. Experimental Design, Materials and Methods

We used the following materials: high purity methane (>99.99 vol% purity, Moscow Gas Refinery Plant, Russia), methanol (≥ 99.7 mass%, Vekton, Russia), monoethylene glycol (≥ 99.7 mass%, EKOS-1, Russia), diethylene glycol (≥ 99.5 mass%, Vekton, Russia), deionized water with the resistivity of 18.2 MΩ·cm (Simplicity UV, Millipore), and Luvicap 55 W (BASF, Germany), a 50 mass% aqueous solution of a vinyl lactam copolymer (1:1 by mol N-vinylpyrrolidone and N-vinylcaprolactam) with a molecular weight of several kDa. The measured n_D^{20} values (Abbemat 650 at D-line, Anton Paar, Austria) for deionized water, methanol, MEG, DEG, and commercial form of kinetic inhibitor Luvicap 55 W were 1.332986 ± 0.000002, 1.328583 ± 0.000006, 1.431723 ± 0.000005, 1.447069 ± 0.000004, and 1.438137 ± 0.000001, respectively. A commercial sample of Luvicap 55 W was freeze-dried. Next, the dry polymer was taken to prepare solutions.

The mass of each aqueous phase sample for measuring methane hydrate equilibrium was 350 g, in the case of rocking cell experiments, 70 g. The components of the aqueous solution were weighed in a conical flask to 0.001 g with a maximum error of ±0.01 g by PA413C balance (Ohaus Pioneer, USA). GHA350 rig (PSL Systemtechnik, Germany) for hydrate equilibrium studies designed for working pressures up to 35 MPa has a volume of 600 mL and includes calibrated pressure, temperature transducers (errors are ±0.02 MPa and ±0.1 K), mixing, and a thermostatic system. The mixing system comprised a four-bladed propeller, a Minipower magnetic coupling (Premex, Switzerland), and an overhead stirrer Hei-TORQUE 400 Precision (Heidolph, Germany). The thermostatic system includes a circulation thermostat CC 505 or Ministat 240 with ethanol (both Huber, Germany) and an outer jacket of the high-pressure cell. Each thermostat can main-

tain the coolant temperature with stability within ±0.02 K. The GHA350 setup is connected to a PC with preinstalled WinGHA software.

The prepared THI solution in the amount of 350 g was placed in a GHA350 high-pressure cell. Air was removed from the free volume of the vessel by flushing with gaseous methane three times (we estimate the residual air content in the gas phase at 0.001–0.002 vol%). The three-phase gas–aqueous solution–hydrate equilibrium in the CH_4–H_2O–THI system was measured by the method described earlier [12,13]. Pressure and temperature of complete dissociation of methane hydrate at slow ramp heating (0.1 K/h) and simultaneous vigorous mixing of fluids (600 rpm) were taken as coordinates of the equilibrium point . For several samples (see caption of Table 1), measurements were made with linear heating at a higher rate (0.5 K/h) or stepwise heating. The outcomes did not differ within the data's uncertainty of temperature and pressure measurements at a heating rate of 0.1 K/h.

The Sapphire Rocking Cells RCS6 (PSL Systemtechnik, Germany) contains six transparent sapphire cells with a volume of 20 mL, which are submerged in a thermostatic bath filled with a water-glycol mixture (coolant) and connected to a thermostat Unistat 510 (Huber, Germany). The RCS6 setup can operate at pressures up to 20 MPa. Each cell has pressure/temperature sensors with an accuracy of ±0.25% and ±0.1 K, respectively. A stainless-steel ball with a diameter of 10 mm is placed in each cell. Its movements from one edge to another can create shear forces when cells are rocking with frequency from 1 to 20 min^{-1} (angle of ± 45°). In this work, the cell rocking frequency was 10 min^{-1}. The movement of the ball facilitates the nucleation of gas hydrates and provides a more efficient mixing of fluids. A PC with WinRCS software controls the RCS6 rig.

Experiments on the nucleation and growth of methane hydrate in the presence of the studied inhibitors were conducted in accordance with the procedure described earlier [14]. The inhibitor solution was placed in each of the six cells of the RCS6 in an amount of 10 mL. Then the cells were closed and installed in the bath. The bath was filled with a coolant, after which the free volume of the cells was purged several times with methane to remove air. The cells were pressurized with gaseous methane to 8.1 MPa at 295 K. The temperature in the bath was set at a level providing hydrate-free thermobaric conditions close to the hydrate phase boundary for the tested sample, and the system was kept for 1 hour. Further, the temperature in the bath decreased at a rate of 1 K/h. After crossing the hydrate phase boundary, the system was in a metastable state (hydrate-free) for some time. Then the process of hydrate formation started and was accompanied by the methane uptake from the gas phase and, as a result, a faster drop in pressure than a linear decrease upon cooling. After the completion of the cooling stage, the temperature in the bath increased to 304–306 K and was kept for 3 h. This led to the dissociation of methane hydrate and the return of the system to the two-phase gas–water solution state. Then the cooling-heating cycles were repeated several times to obtain 12–24 hydrate onset events for each sample. Heating to 304–306 K and keeping for 3 h eliminated the memory effect (formation of hydrate at a higher temperature) in subsequent cooling–heating cycles.

OriginPro 2022b software was used for experimental data processing and visualization.

Ethics Statements

The studies described in the manuscript adhered to Ethics in publishing standards (https://www.elsevier.com/journals/data-in-brief/2352-3409/guide-for-authors) and did not involve human or animal subjects.

Declaration of Competing Interest

The authors declare that they have no known competing financial interests or personal relationships that could have appeared to influence the work reported in this paper.

Data Availability

Dataset for the new insights into methane hydrate inhibition with blends of vinyl lactam polymer and methanol, monoethylene glycol, or diethylene glycol as hybrid inhibitors (Original data) (Mendeley Data).

CRediT Author Statement

Anton P. Semenov: Data curation, Visualization, Validation, Conceptualization, Formal analysis, Methodology, Writing – original draft, Writing – review & editing; **Yinghua Gong:** Investigation; **Vladimir I. Medvedev:** Investigation; **Andrey S. Stoporev:** Visualization, Formal analysis, Writing – original draft, Writing – review & editing; **Vladimir A. Istomin:** Writing – original draft; **Vladimir A. Vinokurov:** Resources, Supervision, Project administration; **Tianduo Li:** Resources, Supervision, Funding acquisition.

Acknowledgments

Funding: Hydrate nucleation and growth studies were supported by the Program for Scientific Research Innovation Team in Colleges and Universities of Shandong Province of Qilu University of Technology (Shandong Academy of Sciences).

Hydrate equilibrium measurements were supported by the Ministry of Science and Higher Education of the Russian Federation under agreement No. 075–15–2022–300 dated 18.04.2022 within the framework of the development program for a world-class Research Center «Efficient development of the global liquid hydrocarbon reserves».

References

[1] A.P. Semenov, Y. Gong, V.I. Medvedev, A.S. Stoporev, V.A. Istomin, V.A. Vinokurov, T. Li, New insights into methane hydrate inhibition with blends of vinyl lactam polymer and methanol, monoethylene glycol, or diethylene glycol as hybrid inhibitors, Chem. Eng. Sci. 268 (2023) 118387, doi:10.1016/j.ces.2022.118387.
[2] H.J. Ng, D.B. Robinson, Hydrate formation in systems containing methane, ethane, propane, carbon dioxide or hydrogen sulfide in the presence of methanol, Fluid Ph. Equilibr. 21 (1985) 145–155, doi:10.1016/0378-3812(85)90065-2.
[3] D.B. Robinson, H.J. Ng, Hydrate formation and inhibition in gas or gas condensate streams, J. Can. Pet. Technol. 25 (1986) 26–30, doi:10.2118/86-04-01.
[4] H. Haghighi, A. Chapoy, R. Burgess, S. Mazloum, B. Tohidi, Phase equilibria for petroleum reservoir fluids containing water and aqueous methanol solutions: experimental measurements and modelling using the CPA equation of state, Fluid Ph. Equilibr. 278 (2009) 109–116, doi:10.1016/j.fluid.2009.01.009.
[5] A.H. Mohammadi, D. Richon, Phase equilibria of methane hydrates in the presence of methanol and/or ethylene glycol aqueous solutions, Ind. Eng. Chem. Res. 49 (2010) 925–928, doi:10.1021/ie901357m.
[6] H. Haghighi, A. Chapoy, R. Burgess, B. Tohidi, Experimental and thermodynamic modelling of systems containing water and ethylene glycol: application to flow assurance and gas processing, Fluid Ph. Equilibr. 276 (2009) 24–30, doi:10.1016/j.fluid.2008.10.006.
[7] A. Chapoy, B. Tohidi, Hydrates in high MEG concentration systems, in: Proceedings of the 3rd Gas Processing Symposium, 2012, pp. 366–373. 10.1016/b978-0-444-59496-9.50050-3.
[8] E. Mahmoodaghdam, Experimental and theoretical investigation of natural gas hydrates in the presence of methanol, ethylene glycol, diethylene glycol and triethylene glycol, J. Phys. Theor. Appl. 1 (2001) 456–459, doi:10.11575/PRISM/24335.
[9] W. Afzal, A.H. Mohammadi, D. Richon, Experimental measurements and predictions of dissociation conditions for methane, ethane, propane, and carbon dioxide simple hydrates in the presence of diethylene glycol aqueous solutions, J. Chem. Eng. Data 53 (2008) 663–666, doi:10.1021/je700457r.
[10] A.H. Mohammadi, D. Richon, Gas hydrate phase equilibrium in methane + ethylene glycol, diethylene glycol, or triethylene glycol + water system, J. Chem. Eng. Data 56 (2011) 4544–4548, doi:10.1021/je2005038.
[11] A.P. Semenov, R.I. Mendgaziev, A.S. Stoporev, V.A. Istomin, D.V. Sergeeva, A.G. Ogienko, V.A. Vinokurov, The pursuit of a more powerful thermodynamic hydrate inhibitor than methanol. Dimethyl sulfoxide as a case study, Chem. Eng. J. 423 (2021) 130227, doi:10.1016/j.cej.2021.130227.
[12] A.P. Semenov, R.I. Mendgaziev, T.B. Tulegenov, A.S. Stoporev, Analysis of the techniques for measuring the equilibrium conditions of gas hydrates formation, Chem. Technol. Fuels Oils. 58 (2022) 628–636, doi:10.1007/s10553-022-01429-w.

[13] Y. Gong, R.I. Mendgaziev, W. Hu, Y. Li, Z. Li, A.S. Stoporev, A. Yu. Manakov, V.A. Vinokurov, T. Li, A.P. Semenov, Urea as a green thermodynamic inhibitor of sII gas hydrates, Chem. Eng. J. 429 (2022) 132386, doi:10.1016/j.cej.2021.132386.

[14] A.P. Semenov, R.I. Mendgaziev, A.S. Stoporev, A.A. Kuchierskaya, A.A. Novikov, V.A. Vinokurov, Gas hydrate nucleation and growth in the presence of water-soluble polymer, nonionic surfactants, and their mixtures, J. Nat. Gas Sci. Eng. 82 (2020) 103491, doi:10.1016/j.jngse.2020.103491.